Influence of H_2O_2 internal motion on scalar and vector properties of OH photofragments

A. U. Grunewald, K.-H. Gericke, and F. J. Comes
Institut für Physikalische und Theoretische Chemie an der Universität Frankfurt am Main, Niederurseler Hang, 6000 Frankfurt am Main, Federal Republic of Germany

(Received 18 March 1988; accepted 25 March 1988)

The formation of ground state OH(X) radicals from the photolysis of jet cooled H_2O_2 at 193 nm is studied by Doppler and polarization spectroscopy. The features of the process are characterized by a complete analysis of the scalar and vector properties of the fragments. In the dissociation process 85% of the available energy is released into fragment translation. The remaining part emerges as rotational excitation that performs a narrow Gaussian-like distribution peaking at $N = 12$ with a FWHM of $\Delta N \cong 5$. The vector correlations between the transition dipole moment μ of the H_2O_2 and recoil velocity v as well as angular momentum J of the products were evaluated in terms of four bipolar moments. The observed $\langle \mu \cdot v \rangle$ correlation was used to determine the state specific contribution of both the $\tilde{A}\,^1A$ and $\tilde{B}\,^1B$ dissociative states to the overall product rotational distribution. On the average, 65% of the OH fragments are formed via the ^1A state. A comparison of data obtained from the photolysis of room temperature and jet cooled H_2O_2 molecules indicates that transfer of parent rotation causes a symmetric broadening of the product distribution and a small increase in the $\langle v \cdot J \rangle$ correlation [$\beta_{vJ}(T \cong 20\ K) = 0.5, \beta_{vJ}(T = 300\ K) = 0.7$] of the fragments. In order to describe the influence of initial parent motion on the product state distribution and on vector correlations a model is used where the formation of two OH radicals in the same microscopic event is considered.

I. INTRODUCTION

Photofragmentation studies under well known initial conditions are an appropriate tool to enlighten chemical events in general. Laser-induced fluorescence is a familiar technique for probing internal state distributions of molecular products. Particularly in connection with classical or quantum scattering calculations, these energy release data provide a deep insight into the mechanism of an elementary chemical step.[1,2] However, this view is limited because it ignores the information related to the anisotropy of the fragmentation process. The disposal of angular momentum and velocity of the photofragments can be determined by spectroscopic methods if the analyzing laser line is sufficiently narrow to resolve the Doppler broadened spectral lines. Each frequency interval within the Doppler profile probes a subset of aligned fragments with velocity components along the laser beam direction. A direct physical interpretation of the relations between parent dipole transition moment μ, fragment velocity v, and angular momentum J can be obtained when the line profile is parametrized with vector correlations.[3–5] With the aid of the directional properties a wealth of information about symmetry, geometry, lifetime, and shape of the dissociative potential energy surface has been obtained.[6–10] The $\langle v \cdot J \rangle$ correlation is a dynamical quantity of great importance because it is only referenced to the molecular frame and, therefore, persists even if there is no directional memory between the photoselected parent molecule and the recoiled fragment as it is the case when the rotational period of parent molecules is short compared to the time of separation.[8–11]

In a supersonic jet experiment the parent molecules are cooled down and the variety of initial states due to thermal excitation is reduced. Furthermore, the fragment velocity is not superimposed on undirected thermal parent velocity but only on a highly directional velocity with a narrow distribution. This type of motion can be ignored in the determination of the vector properties if the laser beams are directed perpendicular to the molecular beam. Thereby the spectral resolution of the experiment is improved.

On the other hand, there is an additional importance of rotationally cooled parent molecules for the evaluation of those vector correlations which are related to the lab frame ($\langle \mu \cdot v \rangle, \langle \mu \cdot J \rangle, \langle \mu \cdot v \cdot J \rangle$ correlations). The molecules will be fixed to some extent to this frame and directional features might appear which are smeared out by rotational or vibrational parent motion.

Moreover, excitation of H_2O in its first absorption band at 157 and 193 nm demonstrates a specific influence of initial parent motion on the fragmentation process. A strong unstatistical Λ-doublet population of the OH fragments was found only when cold parents were photolyzed. This effect was attributed to the conservation of planar symmetry in the absence of parent rotation.[12,13]

In a recent theoretical study the influence of ozone and H_2O parent rotation on O_2 and OH fragment rotational distributions is ascertained. Comparison with experimental data leads to the proposal that minimization of orbital angular momentum dictates which one of the equivalent A–B–A bonds will break in the dissociation process. This corresponds to the constraint that the fragmentation is favored by a product rotational vector $J(AB)$ pointing in the direction

 0021-9606/88/130345-10$02.10

of the vector J(ABA), the parent rotational component perpendicular to molecular plane.[14,15]

Hydrogen peroxide as a four atomic molecule is the simplest example that can execute a torsional motion. Therefore, the $\langle \mathbf{v} \cdot \mathbf{J} \rangle$ correlation is not trivial as it is for triatomic molecules where J is restricted to be perpendicular to v in the high J limit. Any change of the correlation between v and J going from thermal to jet cooled parents reflects the "intrinsic" influence of parent rotation on the fragments. *Ab initio* calculations of the H_2O_2 ground and excited electronic states and the associated transition dipole moments were carried out which allow a determination of the product distribution by classical, or in principle, quantum mechanical calculations.[16–18] Particularly classical trajectory calculations for jet cooled and room temperature H_2O_2 permit a direct comparison with the obtained rotational distributions.[19–21]

From the UV absorption at 266 and 248 nm it was shown that the only excited state is of ^1A symmetry which is the symmetry of the theoretically expected lowest excited electronic state.[9,11] The photolysis wavelength of 193 nm is near the maximum of the first absorption continuum. Since the H_2O_2 absorption spectrum in the region of interest is smooth and monomodal it gives no special hints on the involved transition state(s) but indicates a prompt dissociation process.[22]

The dynamics of the dissociation of room temperature H_2O_2 at 193 nm into two OH radicals has been extensively investigated by photofragment analysis.[10,23,24] The rupture of the O–O bond is induced by transitions from the $\tilde{X}\,^1A$ ground state to the $\tilde{A}\,^1A$ and to the $\tilde{B}\,^1B$ excited states. The fraction of OH radicals formed via the $\tilde{A}\,^1A$ state is 62% while 38% evolve from the $\tilde{B}\,^1B$ state. No significant fragment rotational state specificity for the two fractions was observed. However, there was still an uncertainty in the determination of these fractions due to thermal parent motion. The available energy is exclusively released into translation ($\langle E_{\text{trans}} \rangle = 32\,080$ cm^{-1}) and rotation ($\langle E_{\text{rot}} \rangle = 2780$ cm^{-1}) of the fragments. The rotational excitation can be described by a Gaussian-like distribution peaking at $N = 12$ with a FWHM of $\Delta N \cong 7$. The origin of the rotation was attributed mainly to a strong dihedral dependence of both upper electronic surfaces. This is indicated by a very high $\langle \mathbf{v} \cdot \mathbf{J} \rangle$ correlation of 0.7 corresponding to a more parallel alignment of v and J.

The main goal of the present work is to elucidate the influence of parent rotation on the fragmentation process. Therefore, a complete analysis of the scalar and vector properties is performed in the photolysis of jet cooled hydrogen peroxide. In order to give an explanation for the strong influence of parent motion on the measured fragment properties the microscopic joint probability $P(i,k)$ of forming the two OH fragments in the respective quantum state i and k in a single event is taken into account.[25,26] It was already shown that this probability is strongly influenced by parent rotation about the O–O bond axis which also gives rise to a symmetric broadening of the rotational distribution.

When the parent molecule is "fixed" in the lab frame, as in the present experiment, the $\langle \boldsymbol{\mu} \cdot \mathbf{v} \rangle$ correlation can be predicted if the involved transition moment is known. Vice versa, the measured $\langle \boldsymbol{\mu} \cdot \mathbf{v} \rangle$ correlation will be used to determine the contributions of both simultaneously excited states to the rotational fragment distributions.

II. EXPERIMENTAL

The basic experimental setup is described elsewhere and only the extension including the supersonic jet will be described in detail.[10] Essentially, the dissociating light at 193 nm stemmed from an ArF excimer laser. Resonant fragment excitation was performed by a frequency doubled tunable dye laser pumped by the second harmonic of a Nd:YAG laser. For population measurements the dye laser was tuned in broad band operation (0.5 cm^{-1} FWHM) in the region between 306 and 313.5 nm probing $A\,^2\Sigma^+ \leftarrow X\,^2\Pi_{1/2,3/2}$ transitions of the OH radicals. The LIF signal was viewed perpendicular to the laser beams by a photomultiplier without considering polarization. Doppler profile measurements were carried out with narrow bandwidth ($\sim$0.1 cm^{-1}) probe laser and highly polarized laser radiation. The three different geometries which were used to determine the vector correlations are shown in Fig. 1.

The propagation direction of the jet is aligned along the observation axis of the fluorescence light (x axis in Fig. 1). We used a pulsed nozzle system with aperture of 1 mm diameter and a pulse length of $\sim 200\,\mu$s which was determined by a fast ionization gauge. The mean background pressure in the vacuum chamber was well below 10^{-3} mbar. The interaction region of the two laser beams was set at 1 cm in the case of Doppler profile measurement and at 2 cm for population determination downstream from the nozzle. In order to obtain maximum cooling conditions the photolysis laser pulse was adjusted coincident with the density maximum of the gas pulse. The minimum delay between pump and probe laser was limited by the jitter of the ArF laser and was set to about 50 ns.

The collision rate under free jet expansion conditions is lowered markedly by the cooling effect. However, the still relatively high density in molecular beams has to be taken into account, when photoproducts with high recoil velocity

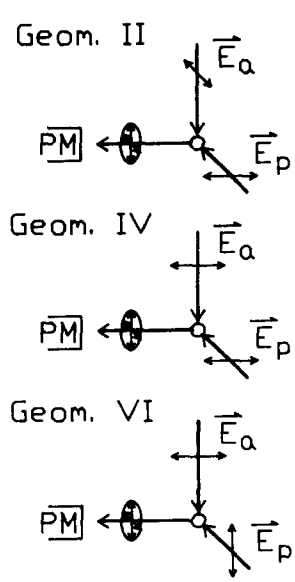

FIG. 1. Characterization of the three different photolysis ($\mathbf{E}_p$) analysis ($\mathbf{E}_a$) detection geometries (II, IV, VI) used to determine the corelations between directed quantities. The propagation of the molecular beam is in direction of the photomultiplier PM.

are to be observed without perturbations by subsequent collisions during the time of interrogation. In order to prove rotational and translational relaxation phenomena the population distribution as well as the Doppler width were monitored at different nozzle stagnation pressures and delay times. We observed very fast translational and even faster rotational fragment relaxation processes.[27] Therefore, optimum nozzle conditions are always a compromise between effective parent cooling and collisions between the fragments and the inert gas. At stagnation pressures of 150 Torr helium nascent OH radicals were observed. The fraction of H_2O_2 seeded in helium was about 1/200.

In order to assess the educt temperature, preceding experiments were carried out with I_2 cooled in jet expansion. Under the same conditions we determined the I_2 rotational temperature to be well below 20 K. Although this will serve only as a rough estimation, the H_2O_2 rotational temperature should be in the same range. The only remarkably depopulated vibrational motion is the relative weak torsional mode. As a reasonable assessment we used a temperature of 150 K in the calculations.

III. RESULTS

To determine the population number in directional specific processes by LIF the dependence of the absorption and fluorescence line intensities on the vector properties has to be taken into account.[4] Fortunately the integrated line intensity is only influenced by the correlation between μ and J which gives rise to a branch specific rotational excitation probability.

In this case, the expression

$$I = CB(q'',q')\nu_0\ P(q'')\,[b_0 + b_1\beta_{\mu J}] \qquad (1)$$

has to be applied to obtain the proper population $P(q'')$ in the quantum state $|q''\rangle$. C is a proportional constant, $B(q'',q')$ are the tabulated B coefficients for absorption, and ν_0 is the center frequency of the transition. The bracket term describes the angular dependence of the intensity I. The multipliers b_0 and b_1 are state, branch, and geometry specific parameters and $\beta_{\mu J}$ is a measure of the $\langle \mu \cdot J \rangle$ correlation which is limited in the range between $+1$ and $-1/2$. Since an average $\beta_{\mu J}$ parameter of 0.05 ± 0.05 was determined, the effect of the alignment is reduced simply by using unpolarized photolysis light. In this case, the error due to the direct conversion of the line intensities into population numbers is less than 2%.

A. Internal state distribution

A scan in the region around 312 nm showed only transitions which were assigned to the $X\,^2\Pi(v''=0) \rightarrow A\,^2\Sigma(v'=0)$ system. Therefore, in the single photon dissociation of jet cooled H_2O_2 at 193 nm the OH fragments are formed vibrationally cold.

The rotational states of $OH(^2\Pi)$ are characterized by the rotational quantum number N describing the electronic and nuclear angular momentum and by J, the *total* angular momentum ($J = N \pm \frac{1}{2}$). The determination of vector properties in any fragmentation process using Doppler and polarization spectroscopy as diagnostic tools is related to the total angular momentum J. Therefore, we will use the symbol J throughout this paper whenever correlations between the rotational motion of the fragment and other vectorial quantities are discussed. However, if the electron spin behaves like a spectator in the dissociation process, it is much more appropriate to describe the fragmention by the rotational quantum number N because in this case populations of states characterized by the same N but different J are comparable while states with the same J but different N exhibit different population numbers.

The fragment spin distribution was analyzed by plotting the ratio

$$R_s = [P(\Pi_{3/2}) - P(\Pi_{1/2})]/[P(\Pi_{3/2}) + P(\Pi_{1/2})]$$

vs the quantum number N of the nuclear rotation (Fig. 2). In order to determine the N tendency we have fitted a second order polynomial to the R_s data. The deviation from $R_s = 0$ which corresponds to an equal population in the spin–orbit states is smaller than 0.05 for each N. Therefore, we assume that no discrimination between the $\Pi_{3/2}$ and $\Pi_{1/2}$ spin–orbit states takes place. The spread in the $R_s(N)$ values may be due to experimental fluctuations.

Since the dissociation process does not distinguish between the spin–orbit states, we used the arithmetic mean over the spin states to calculate the rotational population number $P(N)$ as a function of N. The squares in Fig. 3 represent the rotational distribution formed in the photolysis of jet cooled H_2O_2. For direct comparison the rotational distribution of the corresponding bulk experiment is indicated by the cross symbols.[10] Both distributions peak at $N = 12$. Hence, parent rotation does not induce a shift of the most populated rotational state. The distinguishing feature is the width of the distributions. The bulk data show a FWHM of $\Delta N \cong 7$ while the photolysis of jet cooled H_2O_2 leads to a product distribution with $\Delta N \cong 5$. The solid and the dashed lines plotted in Fig. 3 are the results of classical trajectory calculations[19] and will be discussed later.

Each rotational level of $OH(^2\Pi)$ is Λ doubled. According to a recently recommended notation the $\Pi(A'')$ state which is probed by the Q lines corresponds in the high J limit to an alignment of the $p\pi$ lobe of the unpaired electron along

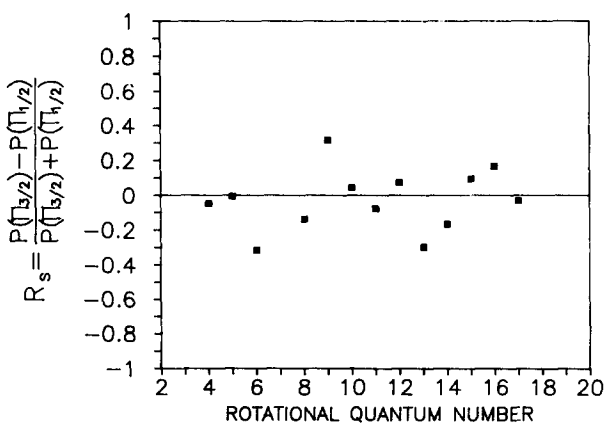

FIG. 2. Product state distribution of the spin–orbit state $^2\Pi_{3/2}$ and $^2\Pi_{1/2}$ as a function of N_{OH}. The different statistical weights have been taken into account.

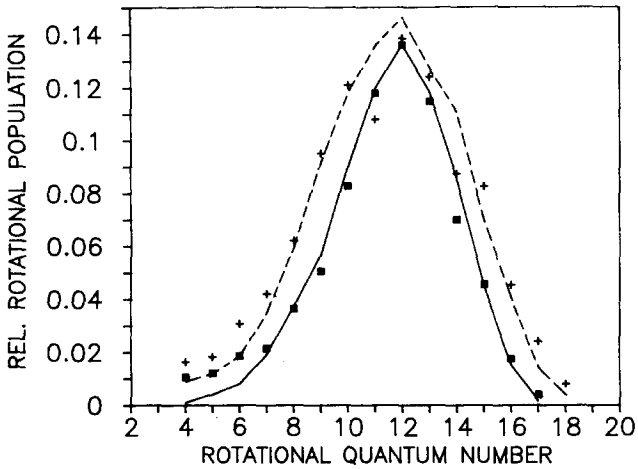

FIG. 3. Relative rotational state population $P(N)$ of the OH fragments as a function of N_{OH} after dissociation of jet cooled (squares) and room temperature (crosses) hydrogen peroxide at 193 nm. The solid and dashed lines are obtained by classical trajectory calculations (Ref. 19). The experimental and theoretical curves are normalized such that the sum of the bulk data as well as the sum of the beam data is equal. For a better comparison the experimental bulk and beam data are normalized at the peaks of the distributions.

the rotational vector **J**, while the electron lobe of the $\Pi(A')$ component lies in the plane of rotation and is detected by P and R transitions.[28] Consequently, the value

$$R_\Lambda = \{P[\Pi(A'')] - P[\Pi(A')]\}/\{P[\Pi(A'')] + P[\Pi(A')]\}$$

reflects the degree of electronic alignment. The limiting values of $R_\Lambda = \pm 1$ which correspond to perfect alignment can only be reached if N goes to infinity. However, for $N > 5$ the condition of the high J limit is fulfilled because the maximum R_Λ value exceeds ± 0.85.[29] In Fig. 4 R_Λ is plotted as a function of N. The solid line is a least square fit of the experimental data to a second order polynominal. For $N < 8$ a small preference for the $\Pi(A')$ component is shown, while for $N > 8$ the $\Pi(A'')$ state is slighly favored in the dissociation process. With the aid of the fitted function and the rotational population $P(N)$ we calculated a weighted mean ratio $\langle R_\Lambda \rangle = \Sigma_N R_\Lambda(N)P(N)$ as a measure of the selectivity of the Λ component in the total process. The value obtained, $\langle R_\Lambda \rangle = 0.049 \pm 0.1$, indicates no preference for one of the Λ components.

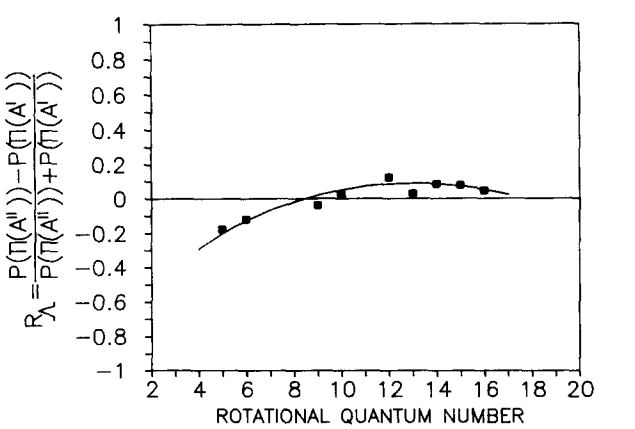

FIG. 4. Product state distribution of the two Λ doublets $\Pi(A'')$, probed by Q lines, and $\Pi(A')$, probed by P lines, as a function of N_{OH}. The solid line is a fitted second order polynomial to the data.

B. Vector correlations

A detailed discussion on vector correlations and their experimental determination is given elsewhere.[4,9,10] Essentially, the experimentally recorded Doppler broadened absorption line is fitted by the function

$$g(x_D) = \frac{1}{2\Delta\nu_D}[1 + \beta_{\text{eff}} P_2(\cos\theta) P_2(x_D)] \qquad (2)$$

with a suitable convolution of laser linewidth and parent thermal motion. $P_2(x) = (3x^2 - 1)/2$ is the second Legendre polynomial. θ is the angle between the E vector of the dissociating light and the propagation direction of the probe laser and $x_D = (\nu - \nu_0)/\Delta\nu_D$ is the relative displacement from the line center ν_0. The parameters to be fitted are the Doppler width $\Delta\nu_D = \nu_0(v/c)$ where v is the average velocity of the very narrow product velocity distribution and β_{eff}, which determines the shape of the Doppler profile and contains all essential information about the vector properties of the dissociation process. In order to extract this information, β_{eff} can be written as a linear combination of three anisotropy parameters $\beta_{\mu v}$, β_{vJ}, and $\beta_{\mu vJ}$. The coefficients of this linear combination depend on the excitation–detection geometry and the branch used for excitation. With a sufficient number of experimentally obtained $\beta_{\text{eff}}(N_{OH})$ values the bipolar moments can be extracted. Moreover, the fit procedure yields the Doppler width which is a measure of the average translational energy of the fragments in each rotational quantum state.

The $\langle \mathbf{v} \cdot \mathbf{J} \rangle$ correlation which is parametrized by β_{vJ} is a dynamical quantity of great importance because it is independent of the lab frame, thereby permitting an insight into fragmentation dynamics directly in the molecular frame. Perfect alignment between **v** and **J** is given when $\beta_{vJ} = +1$ or $\beta_{vJ} = -\frac{1}{2}$ indicating that **v** is either parallel or perpendicular to **J**. All observed rotational states show a significant positive $\langle \mathbf{v} \cdot \mathbf{J} \rangle$ correlation [Fig. 5(b)] which increases with increasing N corresponding to an ascending tendency of **J** being parallel to **v**.

The parameter $\beta_{\mu v}$ which is referenced to the lab frame describes the correlation between the **E** vector of the dissociating light and the velocity vector **v** of the fragments after separation. However, if negligible parent rotation is assumed as in the present jet experiment lab frame and molecular frame are related to each other and $\beta_{\mu v}$ depends only on the angle between the transition dipole moment $\boldsymbol{\mu}$ of the parent molecule and **v**. In Fig. 5(a) the N dependence of the $\beta_{\mu v}$ parameter is shown. The limiting cases of $\beta_{\mu v} = +1$ and $-\frac{1}{2}$ correspond to $\boldsymbol{\mu} \parallel \mathbf{v}$ and $\boldsymbol{\mu} \perp \mathbf{v}$, respectively. The $\langle \boldsymbol{\mu} \cdot \mathbf{v} \rangle$ correlation vanishes for an isotropic process. At lower rotational quantum numbers a minor preference for the dissociation direction perpendicular to $\boldsymbol{\mu}$ was found. Only in the highest observed quantum states the fragmentation direction along $\boldsymbol{\mu}$ is slightly favored [Fig. 5(a)].

The bipolar moment $\beta_{\mu vJ}$ describes the mutual correlation between $\boldsymbol{\mu}$, **v**, and **J**. The limiting numerical values are $\beta_{\mu vJ} = -1$ when all three vectors are either perpendicular to each other or pointing in the same direction and $\beta_{\mu vJ} = +\frac{1}{2}$ in the case when two of the vectors are parallel but perpendicular to the third. Since the spatial distributions

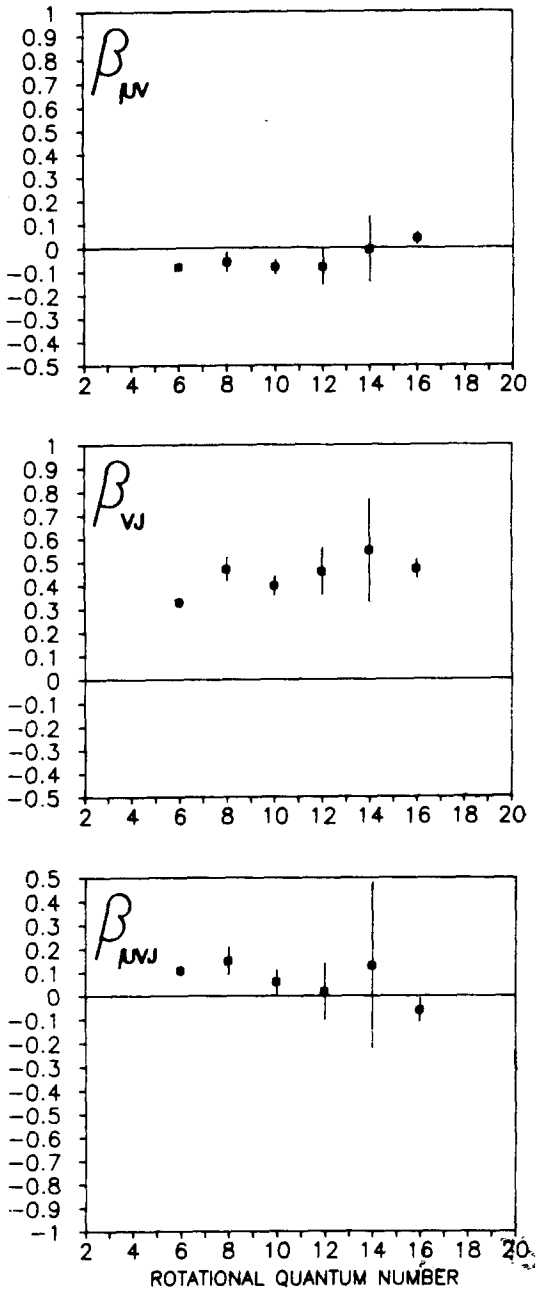

FIG. 5. Observed bipolar moments $\beta_{\mu v}$, β_{vJ}, and $\beta_{\mu vJ}$ as a function of the rotational quantum number N_{OH}. The translational anisotropy of the photofragments is described by $\beta_{\mu v}$. This parameter is used to determine the quantitative contribution of the $\tilde{A}\,^1A$ and $\tilde{B}\,^1B$ potential surfaces to the overall dissociation process. The parameter β_{vJ} characterizes the correlation between the translational and rotational motion of the product. Its positive value increases with increasing fragment rotation indicating a more parallel orientation between J_{OH} and v_{OH}. The low value of $\beta_{\mu vJ}$ describing the correlation between v_{OH}, J_{OH}, and the transition dipole moment μ of the parent is a consequence of the low values for $\beta_{\mu v}$ and $\beta_{\mu J}$, the alignment of the OH product.

of v and J are almost isotropic, it is very unlikely that the fragmentation process is directional with respect to the three vector correlation. Indeed, we found a low value for the $\beta_{\mu vJ}$ parameter of 0.05 ± 0.1 averaged over all observed rotational states. The N dependent values are plotted in Fig. 5(c). They show no significant tendency with the rotational states of the fragment.

In a former study where room temperature H_2O_2 was photolyzed at 193 nm the populations of two dissociating electronic states ($\tilde{A}$,$\tilde{B}$) were probed and the measured product distributions were represented by a superposition of the two distributions originating from the different excited states.[10] With the aid of the calculated dipole transition moment, the individual anisotropy parameters $(\beta_{\mu v})_{A,B}$ of the two fragmentation channels were obtained and the fractional contribution of the two fragmentation channels to the measured product distribution was calculated. However, there was still an uncertainty due to the fact that parent rotation may influence the value of the observed anisotropy parameter because of finite time of separation.

Under the assumption that both excited states lead to fragments with nearly equal velocity $|\mathbf{v}|$ it was shown that the measured parameter $(\beta_{\mu v})_{obs}$ can be expressed as a linear combination of the parameters $(\beta_{\mu v})_A$ and $(\beta_{\mu v})_B$ which are related to the two subprocesses.

The expression

$$(\beta_{\mu v})_{obs} = a(\beta_{\mu v})_A + b(\beta_{\mu v})_B\,, \quad b = 1 - a \qquad (3)$$

yields the fractional contributions a and b of the two channels to the measured product state distribution. For a nonrotating parent molecule the anisotropy parameters for each subprocess A and B, depend only on the involved transition moments $\boldsymbol{\mu}_A = \langle A\,|\boldsymbol{\mu}|X\rangle$ and $\boldsymbol{\mu}_B = \langle B\,|\boldsymbol{\mu}|X\rangle$. Then the $(\beta_{\mu v})_{A,B}$ parameters are simply given by the second Legendre polynomial $P_2(\cos\gamma)$ where γ is the angle between the recoil velocity, which is essentially parallel to the O–O bond axis, and the transition dipole moment $\boldsymbol{\mu}$.

Reinsch[16] investigated in the most recent *ab inito* calculation the excited states of hydrogen peroxide. An essential aim of the work was to carry out a careful calculation of the first three excited electronic states. For energetic reasons it is unlikely that even higher states are involved in the dissociation process at 193 nm. The calculations show that the ground state and the first electronic excited state are of ^1A symmetry. The second as well as the third excited state are of ^1B symmetry. However, only the $\tilde{A}\,^1A$ and the $\tilde{B}\,^1B$ states lead to a rupture of the O–O bond while the second ^1B state is correlated with a break of the O–H bond. The transition moment $\boldsymbol{\mu}_A$ has to be aligned along the C_2 symmetry axis of the molecule ($\gamma_A = 90°$) while $\boldsymbol{\mu}_B$ lies perpendicular to this axis with an angle of $\gamma_B = 4.3°$ to the O–O axis. Therefore, the transition to the $\tilde{A}\,^1A$ state corresponds to a $(\beta_{\mu v})_A$ parameter of -0.5, while a $(\beta_{\mu v})_B$ parameter of $+0.99$ has to be expected for fragmentation via the $\tilde{B}\,^1B$ potential energy surface. Consequently, at 193 nm the H_2O_2 molecule behaves almost like a diatomic molecule where a parallel and perpendicular transition is induced resulting in the fragment distributions $I(\theta)_A \sim \sin^2\theta$ and $I(\theta)_B \sim \cos^2\theta$.

Figure 6 represents the calculated fractional contributions of the two dissociation channels to the population of the fragment quantum states. The small increase with N for the contribution of the $\tilde{B}\,^1B$ state (Fig. 6) was not found when room temperature H_2O_2 was photolyzed. As it will be shown later the parent rotation about the O–O axis adds significantly to the fragment rotation. This effect acts like an averaging process and the contributions of both excited elec-

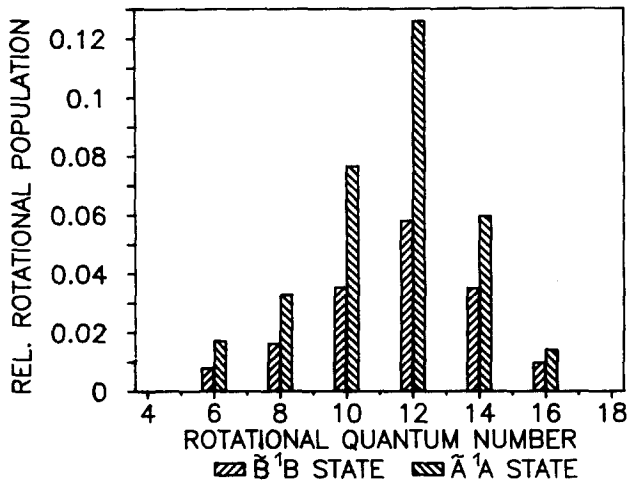

FIG. 6. OH rotational state distribution after excitation of jet cooled hydrogen peroxide in the $\tilde{A}\,^1A$ state or in the $\tilde{B}\,^1B$ state.

tronic states to a specific fragment rotational state are smeared out over several states by parent rotation. In total, 65% of the OH fragments are formed via the $\tilde{A}\,^1A$ state and 35% result from excitation of the $\tilde{B}\,^1B$ state.

C. Energy partitioning

The distribution of the energy released in the dissociation process over the various degrees of freedom of the fragments is governed by the shape of the excited potential energy surface and the initial conditions in the parent molecule. The total excess energy E_{av}, which is available to the photofragments, is determined by the dissociation energy E_d, the photon energy $h\nu = 619.1$ kJ/mol, and the internal energy of the parent molecule $E_{\rm int}(H_2O_2)$:

$$E_{\rm av} = h\nu + E_{\rm int}(H_2O_2) - E_d \,. \tag{4}$$

The internal energy of the jet cooled parent molecule is not exactly known. We assume a rotational temperature of $T_{\rm rot} = 20$ K and a vibrational temperature of $T_{\rm vib} = 150$ K which results in an internal energy of $E_{\rm int}(H_2O_2) = 0.8$ kJ/mol.

The available energy emerges in the fragments as rotational and translational excitation. Since the Doppler profile measurements yield the mean kinetic energy $\langle E_{\rm kin}(N)\rangle$ of all fragments in a specific rotational state, we obtain

$$E_{\rm av} = 2\sum_N P(N)E_{\rm rot}(N) + 2\sum_N P(N)\langle E_{\rm kin}(N)\rangle \,, \tag{5}$$

where $P(N)$ is the normalized rotational population and the factor 2 is a consequence of the fact that two OH radicals are formed in each elementary process. With $E_{\rm av} = 422.55$ kJ/mol, the dissociation energy can be determined by spectroscopic means to be $E_d = 197.4$ kJ/mol. The uncertainty due to parent temperature will not significantly alter this result because of the minor contribution from the internal parent energy. The same calculation was done with data obtained in bulk experiments at the photolysis wavelengths of 266 and 193 nm resulting in dissociation energies of 194 and 199 kJ/mol, respectively.[26]

The fraction of energy which is transferred into OH rotation is given by $f_{\rm rot} = 2\,\Sigma_N P(N)E_{\rm rot}(N)/E_{\rm av} = 0.15$. Consequently, the fraction of energy emerging in fragment translation is $f_{\rm kin} = 2\,\Sigma_N P(N)\langle E_{\rm kin}(N)\rangle/E_{\rm av} = 0.85$. Within the experimental uncertainty similar results had been obtained in the photolysis of thermal H_2O_2 in bulk experiments at 193 nm.[10,23,24]

IV. THE DISSOCIATION PROCESS

The photolysis of jet cooled H_2O_2 at 193 nm results in an almost isotropic OH product velocity distribution. With the aid of the calculated dipole transition moments of the first and second electronic excited states this distribution can be explained when a contribution of 0.65 for the $\tilde{A}\,^1A$ state and 0.35 for the $\tilde{B}\,^1B$ state to the absorption cross section is assumed. The total absorption cross section of H_2O_2 at 193 nm may also include small contributions of the excitation of the $\tilde{C}$ state resulting in the break of the O–H bond and the production of H atoms which cannot be observed in the present experiment.[16,30]

Nuclear fragmentation in two OH radicals evolves separately on two potential energy surfaces, however, the internal excitation of fragments formed via the different surfaces is quite similar. No vibrational excitation was found and the rotational distributions originating from the $\tilde{A}\,^1A$ and $\tilde{B}\,^1B$ state are peaking at the same rotational quantum number and show a comparable shape (Fig. 6). Consequently, the translational energy released in the different process has to be almost the same.

The analysis of the $\langle \mathbf{v}\cdot\mathbf{J}\rangle$ correlation can elucidate these surprising results. We found a strong positive correlation of about 0.5 for all fragment quantum states pointing out that an alignment of **J** being parallel to **v** is significantly favored. In the absence of parent rotation the **v** vector is strictly related to the molecular frame. In this frame the separation coordinate is given by the vector **R** which joins the center of mass of the OH rotors. Because of the mass distribution **R** is almost in the O–O bond axis.

For high rotational quantum numbers a classical momentum representation permits a more vivid view of the dynamics of the fragmentation process. In a body-fixed coordinate system where the transition dipole moments μ_A as well as μ_B define the z axis the recoil velocity **v** of fragments formed via the $\tilde{A}\,^1A$ state will be aligned perpendicular to the z axis and thus define, e.g., the x axis. When the $\tilde{B}\,^1B$ state, treated as a parallel transition, is excited **v** will be aligned along the z axis. The observed bipolar moments $(\beta_i)_{\rm obs}$ are the weighted sum of the corresponding bipolar moments related to the respective transition state

$$(\beta_i)_{\rm obs} = a(\beta_i)_A + (1-a)(\beta_i)_B \,. \tag{6}$$

In the coordinate system defined above these bipolar moments can be expressed by the expectation values of the square components of the angular momentum referring to the proper transition state

$$2J_A(J_A+1)(\beta_{\mu J})_A = 2\langle J_z^2\rangle_A - \langle J_x^2\rangle_A - \langle J_y^2\rangle_A \,, \tag{7}$$

$$2J_A(J_A+1)(\beta_{\omega J})_A = 2\langle J_x^2\rangle_A - \langle J_y^2\rangle_A - \langle J_z^2\rangle_A \,, \tag{8}$$

$$2J_A(J_A+1)(\beta_{\mu\nu J})_A = \langle J_x^2\rangle_A + \langle J_z^2\rangle_A - 2\langle J_y^2\rangle_A \,, \tag{9}$$

$$2J_B(J_B+1)(\beta_{\mu J})_B = 2\langle J_z^2\rangle_B - \langle J_x^2\rangle_B - \langle J_y^2\rangle_B , \quad (10)$$

$$(\beta_{\omega J})_B = -(\beta_{\mu\omega J})_B = (\beta_{\mu J})_B . \quad (11)$$

Equations (6)–(11) were used to determine the bipolar moments $(\beta_i)_A, (\beta_i)_B$ and the expectation values of the squared angular momentum components. Table I contains the observed bipolar moments ($N \geqslant 14$) and the calculated state specific bipolar moments and expectation values of the squared J components.

The bipolar moments $(\beta_{\omega J})_A$ and $(\beta_{\omega J})_B$ describing the $\langle \mathbf{v} \cdot \mathbf{J} \rangle$ correlation are both positive. Therefore, the major part of the rotational energy ($\langle E_{\rm rot} \rangle = 2735.9\ {\rm cm}^{-1}$) is released via torsional motion in the OH rotor. If we would assume that *no* torque is induced by final state interaction, then almost 50% of the mean vibrational energy of the parent molecule (including zero point energy) can be transferred into product rotation.[31,32] The energy which one OH fragment receives from the torsional mode of the parent H_2O_2 is calculated to be 47 cm^{-1}. Therefore, the strong dihedral angle dependence of both upper potential surfaces is the main origin of fragment rotation. Quantitatively, the $\langle J_x^2\rangle_A = 0.69$ and the $\langle J_z^2\rangle_B = 0.63$ expectation values describe that part of fragment rotational energy induced by the dihedral angle dependence of the upper potential surfaces.

The contributions from parent bending modes (almost exclusively zero point) to the fragment rotation will emerge in the $\langle J_y^2\rangle_A + \langle J_z^2\rangle_A = 0.31$ and $\langle J_x^2\rangle_B + \langle J_y^2\rangle_B = 0.37$ components. We calculate that the zero point energy of the parent bending modes adds a fraction of 0.12 (331 cm^{-1}) to the rotational energy of one OH fragment. Both upper potential energy surfaces should only show a weak dependence along the bending coordinates.

Recently Meier *et al.* calculated the potential energy surfaces of the $\tilde{A}\ ^1A$ and $\tilde{B}\ ^1B$ states by quantum mechanical *ab initio* methods.[17] The torsional dependence of the electronic ground state and the first two excited states is schematically shown in Fig. 8 (right part). The ground state potential function was evaluated on the basis of the hindered potential function.[33] A Franck–Condon transition from the zero point level of the ground state to the $\tilde{A}\ ^1A$ state results in a torque with a direction of rotation to the *trans* configuration while an excitation of the $\tilde{B}\ ^1B$ state induces a torque to the *cis* configuration. The shape of the torsional dependence of both excited states in the Franck–Condon region is nearly the same which explains the comparability of the rotational distributions of the fragments evolving on the different upper potential surfaces.

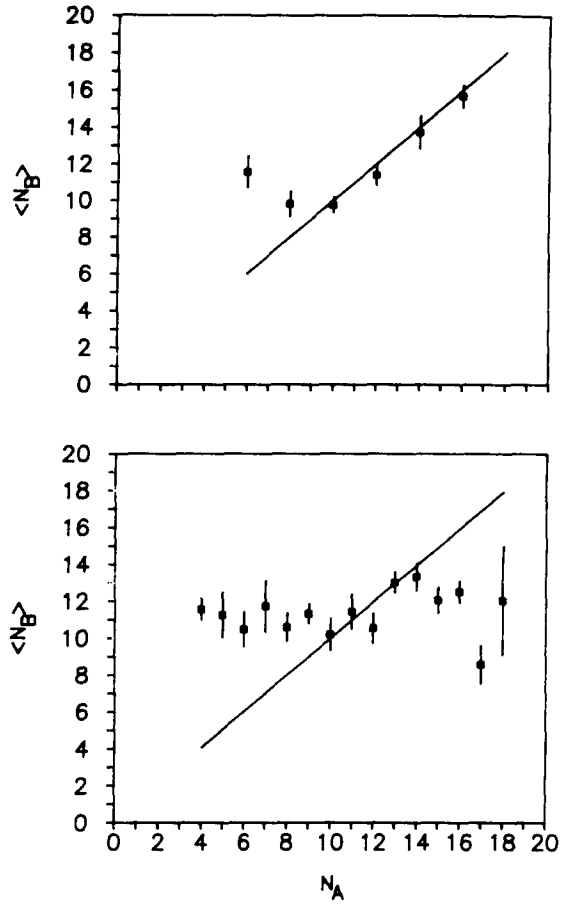

FIG. 7. Correlation between the rotation of the two OH partner products OH_A and OH_B formed in the same dissociation process of jet cooled (upper part) and room temperature hydrogen peroxide, $H_2O_2 + h\nu(193\ {\rm nm}) \rightarrow OH_A + OH_B$. Due to the limited resolution of the analyzing dye laser only the mean partner rotation $\langle N_B \rangle$ can be determined as a function of the rotational quantum number N_A of molecules OH_A formed in this state.

Schinke and Staemmler examined the photodissociation of cold and room temperature H_2O_2 at 193 nm using classical trajectory calculations on the *ab initio* potential energy surfaces of the two lowest excited states ($\tilde{A}\ ^1A$ and $\tilde{B}\ ^1B$).[19] The two separate fragment rotational distributions formed via the $\tilde{A}$ and $\tilde{B}$ state were averaged according to the ratio of 0.7:0.3 which was obtained using the respective dipole transition moments calculated by Reinsch.[16] An initial parent rotational temperature of 50 K and no vibrational hot band excitation was assumed. The resulting fragment distribution shown in Fig. 3 (solid line) is in remarkable agreement with the measured data of the jet cooled experiment. The separate

TABLE I. Bipolar moments β_i and expectation values of the squared angular momentum components. The transition dipole moment in the parent H_2O_2 defines the z axis. The recoiling OH fragments move essentially along this axis if they are formed via the $\tilde{B}\ ^1B$ repulsive state. Those fragments which are generated via the $\tilde{A}\ ^1A$ state move perpendicular to the z axis. The observed moments $(\beta_i)_{\rm obs}$ were taken for high OH rotations ($N > 14$) to evaluate the vector correlations for excitation of the $\tilde{A}\ ^1A$ and $\tilde{B}\ ^1B$ state.

	$\beta_{\mu J}$	$\beta_{\mu v}$	β_{vJ}	$\beta_{\mu vJ}$	$\langle J_x^2\rangle$	$\langle J_y^2\rangle$	$\langle J_z^2\rangle$
$(\beta_i)_{\rm obs}$	0.02	0.0	+0.51	+0.04			
$\tilde{A}\ ^1A$	−0.5	−0.24	+0.54	+0.30	0.69	0.13	0.18
$\tilde{B}\ ^1B$	+1.0	+0.45	+0.54	−0.45	0.37		0.63

rotational distributions are shifted by only one quantum number. The calculations on the $\tilde{A}$ surface yield the maximum population for the $N = 12$ state while the population formed via the $\tilde{B}$ state is peaking at $N = 11$.

We found that the major part of fragment rotation ($\sim 66\%$) is induced via the torsional coordinate. This implies that there is a correlation between the rotational quantum numbers of the two partner molecules (N_A, N_B) formed coincidently in one elementary step because for rotational vectors $\mathbf{N}_A$ and $\mathbf{N}_B$ which are aligned parallel to the direction of separation, the relation $\mathbf{N}_A = -\mathbf{N}_B$ has to hold.[25,26] This corresponds to a correlation between angular momenta of coincident product pairs formed in one elementary fragmentation process. The subscripts A and B refer to the product partner molecules OH_A and OH_B formed in an elementary process and should not be mistaken with the identification of the upper potential energy surfaces $\tilde{A}\,^1A$ and $\tilde{B}\,^1B$. A comprehensive discussion on correlation between partner products and preliminary results obtained in the photolysis of room temperature and jet cooled H_2O_2 at 193 nm and $H_2O_2(D_2O_2)$ at 266 nm can be found elsewhere.[25,26] In short, each elementary fragmentation leads to two OH radicals which may be formed in two different rotational quantum states $|i\rangle$ and $|k\rangle$. The elements of the matrix $P(i,k)$ represent the joint reaction probabilities of these microscopic events. Then the measured population of a rotational level $|i\rangle$ can be expressed as the sum $P(i) = \Sigma_k P(i,k)$. The conservation of energy and linear momentum in a fragmentation where the OH partner fragments A and B are formed demands:

$$E_{\mathrm{rot}}(\mathrm{B}) = \mathrm{E}_{\mathrm{rot}}(\mathrm{A}) - E_{\mathrm{av}} + mv^2 . \qquad (12)$$

The kinetic energy of the observed OH radical reflects the rotational energy $\mathrm{E}_{\mathrm{rot}}(\mathrm{B})$ of the partner fragment B. When an ensemble of fragments is analyzed the resulting Doppler profile for a particular transition starting at a specific rotational quantum state can be written as a sum of single profiles with the same center frequency but different Doppler widths and weighting factors $P(i,k)$. Thereby the population $P(i,k)$ of the quantum state $|k\rangle$ is probed and identified by the respective kinetic energy (Doppler width) which permits, in principle, a determination of the matrix $P(i,k)$.

The linewidth of the analyzing dye laser is not sufficiently narrow to resolve the structure hidden in the Doppler profiles, produced by the different states of the partner molecule. However, we observed the average Doppler width for each rotational state of OH_A and thereby the average rotational energy $\langle E_{\mathrm{rot}}(\mathrm{B})\rangle$ of the partner molecule. These energies can be converted into rotational quantum numbers. Figure 7 shows a plot of the rotational quantum number N_A of molecules A vs the correlated mean rotational quantum number $\langle N_B\rangle$ of their partners B. When jet cooled parent molecules are photolyzed (upper part of Fig. 7) the rotational quantum number N_A is highly correlated with the averaged rotational quantum number $\langle N_B\rangle$ of the partners ($N_A \cong N_B$). This indicates, again, the dominating contribution of torsional motion of the OH rotors to the total rotational motion. Only at quantum numbers $N_A < 10$ a significant deviation from the bisecting line was observed. This deviation can be explained by contributions from parent zero point bending motion and the bending angle dependence of the upper potential surfaces to the fragment rotation. For this type of motion the orbital angular momentum $\mathbf{L}_{AB}$ of the OH center of mass relative to each other can fulfill the conservation of angular momentum $\mathbf{N}_A + \mathbf{N}_B + \mathbf{L}_{AB} = 0$.

V. THE INFLUENCE OF PARENT ROTATION

As far as the energetic aspect is concerned there is no significant difference between the photolysis of jet cooled and room temperature H_2O_2 at 193 nm. The relative weak temperature dependence indicates by itself that the product state distribution is mainly determined by strong final state interaction. However, the small thermal parent excitation compared to the available energy of the dissociation process does not necessarily mean that the initial conditions of the parent molecule are of minor importance. The most interesting effect of parent thermal excitation appears in the directional properties of the fragments as well as in the width of the fragment rotational distribution and in the microscopic joint reaction probability $P(i,k)$. This wealth of information establishes a detailed picture of the transfer of parent motion into fragment rotation.

The thermal parent translational motion can be neglected in the c.m. system. In the lab system it slightly increases the spread of the resulting OH product velocity distribution. Thereby it affects only the spectral resolution in the experiment to a minor extent but not the observed OH properties itself.

The only contribution to vibrational excitation at 300 K stems from the ν_4 torsional mode of the parent molecule. The energy stored in the excited states of this mode is very small compared to the mean OH rotational energy ($\sim 2\%$). Since energy transfer from this mode will act in the same way as the torsional angle dependent final state interaction does, we do not assume an observable contribution from this part of the thermal energy on the product properties. Also a favored hot band excitation is unlikely because the measured ratio of the partial absorption cross sections of the $\tilde{A}\,^1A$ and $\tilde{B}\,^1B$ excited states are very similar when room temperatures and jet cooled H_2O_2 is photolyzed.

In order to evaluate the effect of parent rotation on the OH fragment properties one has to distinguish between the rotation about the three different axes of inertia. The rotational vector $\mathbf{N}_R$ of the parent H_2O_2 parallel to the vector $\mathbf{R}$ has to be superimposed almost exclusively on the fragment rotation induced by final state interaction because no orbital angular momentum can be expected if the ground state geometry and the mass relation are taken into account. This situation is illustrated in Fig. 8 where product rotation is assumed to originate exclusively from the torsional angle dependence of the upper potential surface with the superposition of parent rotation $\mathbf{N}_R$. In this case the final OH rotation $N_f(\mathrm{OH})$ is given by $N_f(\mathrm{OH_A}) = N(\mathrm{OH_A}) + N_R$ for one OH product and $N_f(\mathrm{OH_B}) = N(\mathrm{OH_B}) - N_R$ for the partner fragment. The mean thermal rotation energy $\frac{1}{2}kT$ corresponds to a parent rotation of $N_R \cong 3\hbar$ resulting in a

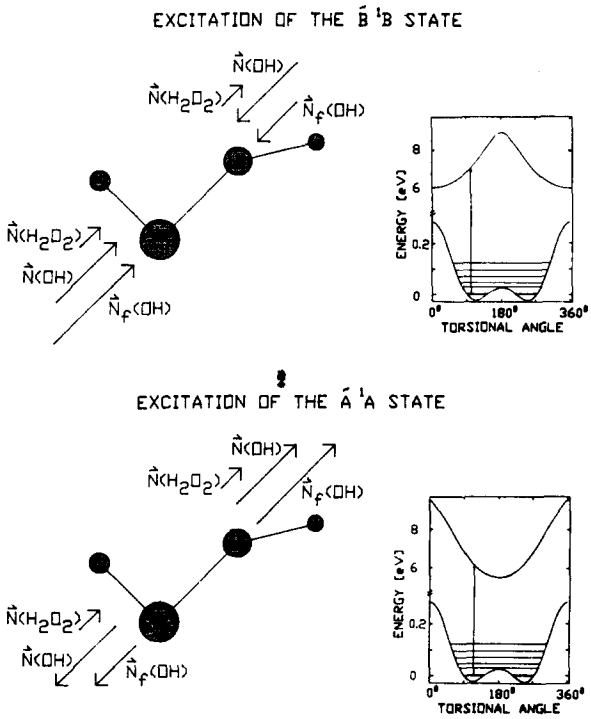

FIG. 8. OH product rotation induced by the torsional dependence of the upper potential surface. The $\tilde{A}\,^1A$ state has its lowest energy in a *trans* configuration while the $\tilde{B}\,^1B$ state strongly favors a *cis* configuration. The torque on the OH rotor induced by final state interaction N(OH) is influenced by parent rotation $N(H_2O_2)$, resulting in a final OH fragment rotation $N_f(OH)$, where the partner products are released with different angular momentum.

difference of the rotation of the partner molecules $\Delta N_f = N_f(OH_A) - N_f(OH_B) \cong 6\hbar$

For rotation induced via bending like motion of the OH rotor the final OH rotation $N_f(OH)$ will be influenced mainly in its direction because in this case N(OH) is essentially aligned perpendicular to N_R.

The angular momentum of the parent molecule about the two other axes of inertia perpendicular to N_R will be transferred to a major extent only into orbital angular momentum $L_{AB} = \mu_{AB} b v_0$ where μ_{AB} is the reduced mass of the OH partner fragments and b is an impact parameter. Thereby the velocity v_0 will slightly increase the final velocity of the fragments.

When jet cooled H_2O_2 was photolyzed we found for fragment rotational quantum number $N > 8$ that both partner radicals are formed with the same quantum number $N_A \cong N_B$. Corresponding investigations were performed for the dissociation of room temperature H_2O_2 with the surprising result that this strong correlation breaks down (lower part of Fig. 7). The data obtained in the bulk experiment show a strong deviation from the bisecting line representing the case of $N_A = N_B$. Therefore, fragments formed in any rotational state have on the average partners with medium angular momentum. This behavior can only be attributed to the influence of parent rotation. In particular the parent rotation about the **R** axis results in a difference in the final quantum number of the partner molecules of $\Delta N_f(OH) = 2N_R$(parent). With average parent angular momentum of $N_R = 3\hbar$ at $T = 300$ K a fragment formed at, e.g., $N_f(OH) = 18$ has a partner at $N_f(OH) = 12$ while a fragment in the quantum state $N_f(OH) = 4$ has a partner at $N_f(OH) = 10$. This shows that the small amount of parent thermal excitation compared with the total energy released in the dissociation process can strongly influence the microscopic joint reaction probability $P(i,k)$.

The qualitative picture of the effect of parent rotation implies that the product state distribution formed in the photolysis of room temperature H_2O_2 can be calculated by a convolution of the product state distribution obtained from jet cooled H_2O_2 with the rotational population of the parent molecule (rotation about the O–O axis). This convolution results in an almost *symmetric* broadening of the rotational OH product state distribution formed by final state interaction as it was observed when room temperature H_2O_2 was photolyzed.

Schinke and Staemmler investigated quantitatively the photodissociation of H_2O_2 at 193 nm according to the procedure described in Sec. IV but assuming thermal initial parent conditions with a temperature of 300 K.[19] The resulting product distribution shown in Fig. 3 (dashed line) is in good agreement with the measured bulk data.

The thermal excitation of the parent molecule affects the measured $\langle \mathbf{v} \cdot \mathbf{J} \rangle$ correlation in an unexpected way. At medium rotational quantum numbers of the photofragments the $\langle \mathbf{v} \cdot \mathbf{J} \rangle$ correlation from room temperature H_2O_2 $\beta_{vJ}(T = 300\text{ K})$, is comparable with the data from the jet cooled experiment $\beta_{vJ}(T \cong 20\text{ K})$. At the lowest observed quantum number $N = 4$ the parameter $\beta_{vJ}(T = 300\text{ K})$ approaches zero. This behavior was not found in the jet cooled experiment. However, due to the very small population number we could not perform precise Doppler profile measurements at quantum numbers below $N = 6$ in the jet experiment. At high quantum numbers the influence of parent thermal exitation becomes obvious. The ratio of the β_{vJ} parameters in this region is β_{vJ} $(T = 300\text{ K})/\beta_{vJ}(T \cong 20\text{ K}) = 0.7/0.5$ indicating an increase of the $\langle \mathbf{v} \cdot \mathbf{J} \rangle$ correlation induced by parent thermal motion.

The classical definition of $\beta_{vJ} = \langle (3(\mathbf{v} \cdot \mathbf{J}/vJ)^2 - 1)/2 \rangle = 0.5$ yields an average angle between $\mathbf{v} \| \mathbf{R}$ and N(OH) of $\cong 35°$ in the photofragmentation of jet cooled H_2O_2. An increase of the $\langle \mathbf{v} \cdot \mathbf{J} \rangle$ correlation corresponds to an additional angular momentum aligned parallel to **v**. The model of transfer of parent rotation into fragment rotation implies that the highest observed quantum numbers $N_f(OH)$ in the bulk experiment are given by $\mathbf{N}_f(OH) = \mathbf{N}(OH) + \mathbf{N}_R$. With $\mathbf{N}_R = 3\hbar\,\mathbf{R}/R$ and, e.g., $N(OH) = 14$ we calculated an angle of 29° between $\mathbf{N}_f(OH)$ and **v**. The agreement with the measured angle in the bulk experiment of 26° is a further hint on the correctness of the qualitative transfer picture of parent rotation and explains how a random thermal motion can increase a directional property of the dissociation process.

VI. CONCLUSION

In the present paper we demonstrate that polarization and Doppler spectroscopy in combination with the supersonic jet technique enables a deeper insight into photodisso-

ciation. The near absence of parent rotation allows that lab frame referenced vector correlations can be interpreted more directly in terms of the molecular frame. When hydrogen peroxide is photolyzed at 193 nm the quantitative contributions of the first two dissociative electronic states were directly calculated from the measured $\langle \mu \cdot v \rangle$ correlation with the aid of *ab initio* calculated dipole transition moments. The relative contributions of the $\tilde{A}\,^1A$ and $\tilde{B}\,^1B$ states to the total OH production were determined to be 0.65 and 0.35, respectively.

An intrinsic influence of parent rotation on all important fragment properties was observed. A symmetric broadening of the fragment rotational distribution is caused by parent rotation about the O–O axis. A slightly lower $\langle v \cdot J \rangle$ correlation was obtained in the jet cooled experiment than in the bulk experiment. This increase is attributed to a transfer of parent rotation inducing a supplemental angular momentum mainly in the direction of fragment separation. The result of the bulk experiment that fragment rotation is primarily induced by the strong dihedral angle dependence of both upper electronic surfaces is confirmed.

The important correlation of the angular momenta of both fragments formed in a single dissociation event $[N(OH_A), N(OH_B)]$ is strongly influenced by parent rotation. We observed the correlation $N(OH_A) \cong N(OH_B)$ at quantum states $N > 8$ while the bulk data show only a weak correlation. This result is obviously not based on an exact proof because the spectral resolution of the probe laser permits only the determination of the average angular momentum of the partner molecule. Experiments with an improved resolution are in progress which will allow a measurement of the state resolved partner distribution.

ACKNOWLEDGMENTS

The work has been performed as part of a program of the Deutsche Forschungsgemeinschaft (DFG). Financial support by the DFG and the Fonds der Chemischen Industrie is gratefully acknowledged. We thank R. Schinke and V. Staemmler for stimulating discussions and for sending results of their calculations prior to publication.

[1]W. M. Jackson and H. Okabe, Adv. Photochem. **13**, 1 (1986).
[2]M. N. R. Ashfold and J. E. Baggot, *Molecular Photodissociation Dynamics* (Royal Society of Chemistry, London, 1987).
[3]C. H. Greene and R. N. Zare, Annu. Rev. Phys. Chem. **33**, 119 (1982); J. Chem. Phys. **78**, 6741 (1983).
[4]R. N. Dixon, J. Chem. Phys. **85**, 1866 (1986).
[5]G. E. Hall, N. Sivakumar, P. L. Houston, and I. Burak, Phys. Rev. Lett. **56**, 1671 (1986).
[6]J. Solomon, C. Jonah, P. Chandra, and R. Bersohn, J. Chem. Phys. **55**, 1908 (1971); C. Jonah, *ibid.* **55**, 1915 (1971).
[7]G. E. Busch and K. R. Wilson, J. Chem. Phys. **56**, 3638, 3655 (1972).
[8]S. Klee, K.-H. Gericke, and F. J. Comes, J. Chem. Phys. **85**, 40 (1986).
[9]K.-H. Gericke, S. Klee, F. J. Comes, and R. N. Dixon, J. Chem. Phys. **85**, 4463 (1986); K.-H. Gericke, Faraday Discuss. Chem. Soc. **82**, 41 (1986).
[10]A. U. Grunewald, K.-H. Gericke, and F. J. Comes, J. Chem. Phys. **87**, 5709 (1987).
[11]M. P. Docker, A. Hodgson, and J. P. Simons, Chem. Phys. Lett. **128**, 264 (1986); Faraday Discuss. Chem. Soc. **82**, 25 (1986).
[12]P. Andresen, G. S. Ondrey, B. Titze, and E. W. Rothe, J. Chem. Phys. **80**, 2548 (1984).
[13]A. U. Grunewald, K.-H. Gericke, and F. J. Comes, Chem. Phys. Lett. **133**, 501 (1987).
[14]H. B. Levene, J.-L. Nieh, and J. J. Valentini, J. Chem. Phys. **86**, 2583 (1987).
[15]H. B. Levene and J. J. Valentini, J. Chem. Phys. **86**, 2594 (1987).
[16]E. A. Reinsch, Chem. Phys. Lett. **141**, 369 (1987).
[17]U. Meier, V. Staemmler, and J. Wasilewski (to be published).
[18]L. Cheraldonnet, H. Lardy, and A. Dargelos, Chem. Phys. **102**, 55 (1986).
[19]R. Schinke and V. Staemmler, Chem. Phys. Lett. **145**, 486 (1988).
[20]R. Schinke, V. Engel, S. Hennig, K. Weide, and A. Untsch, Ber. Bunsenges. Phys. Chem. **92**, 295 (1988).
[21]R. Schinke, in *Collision Theory for Atoms and Molecules*, edited by F. Gianturco (Plenum, New York, 1988).
[22]L. T. Molina and M. J. Molina, J. Photochem. **15**, 97 (1981); M. Suto and L. C. Lee, Chem. Phys. Lett. **98**, 152 (1983).
[23]A. U. Grunewald, K.-H. Gericke, and F. J. Comes, Chem. Phys. Lett. **132**, 121 (1986).
[24]A. Jacobs, M. Wahl, R. Weller, and J. Wolfrum, Appl. Phys. B **42**, 173 (1987).
[25]K.-H. Gericke, Phys. Rev. Lett. **60**, 561 (1988).
[26]K.-H. Gericke, A. U. Grunewald, S. Klee, and F. J. Comes, J. Chem. Phys. **88**, 6255 (1988).
[27]A. U. Grunewald, K.-H. Gericke, and F. J. Comes (to be published).
[28]M. H. Alexander, P. Andresen, R. Bacis, R. Bersohn, F. J. Comes, P. J. Dagdigian, R. N. Dixon, R. W. Field, G. W. Flynn, K.-H. Gericke, E. R. Grant, B. J. Howard, J. R. Huber, D. S. King, J. L. Kinsey, K. Kleinermanns, K. Kuchitsu, A. C. Luntz, A. J. McCaffery, B. Pouilly, H. Reisler, S. Rosenwaks, E. W. Rothe, M. Shapiro, J. P. Simons, R. Vasudev, J. R. Wiesenfeld, C. Wittig, and R. N. Zare (to be published).
[29]P. Andresen and E. W. Rothe, J. Chem. Phys. **82**, 3634 (1985).
[30]U. Gerlach-Meyer, E. Linnebach, K. Kleinermanns, and J. Wolfrum, Chem. Phys. Lett. **133**, 113 (1987).
[31]M. D. Morse and K. F. Freed, J. Chem. Phys. **78**, 6045 (1983); M. D. Morse, Y. B. Band, and K. F. Freed, *ibid.* **78**, 6066 (1983).
[32]H. Gölzenleuchter, K.-H. Gericke, F. J. Comes, and P. F. Linde, Chem. Phys. **89**, 93 (1984).
[33]R. H. Hunt, R. A. Leacock, C. W. Peters, and K. T. Hecht, J. Chem. Phys. **42**, 1931 (1965); R. Block and L. Jansen, *ibid.* **82**, 3322 (1985).